DOI:10.1190/segam2020-3427923.1

# Iterative least-squares migration for high-resolution angle gathers

*Lian Duan*, Alejandro Valenciano, Nizar Chemingui, PGS*

**Summary**

Seismic amplitudes can be biased by uneven illumination in the presence of a complex overburden. Iterative Least-Squares Migration (LSM) can reduce the amplitude bias and improve the resolution of the images. We introduce a robust and practical iterative least-squares migration for the inversion of angle domain common image gathers. The algorithm uses wave-equation migration and demigration in the extended subsurface offset domain followed by an offset to angle transformation. We demonstrate using the Sigsbee2b synthetic and field data from Santos Basin, offshore Brazil that iterative LSM provides high-resolution angle domain common image gathers, extending their usable angle range, and balancing their amplitudes.

**Introduction**

Earth models, acquisition parameters, and imaging operators can affect seismic amplitudes fidelity. The bias is particularly prominent in the presence of complex overburden, impacting the interpretation of amplitudes variability with angle (AVO/AVA). To resolve the problem, the framework of Least-Squares Migration (LSM), seeks an inverted reflectivity image that minimizes the difference between the modeled and recorded data. Recently, LSM has become the high-end imaging tool of choice. Most algorithms rely on low rank approximations of the inverse least-squares Hessian (Guitton, 2004) or sparse of the Hessian computation in a grid of point scatters (Valenciano et al., 2019). However, a practical and stable formulation of iterative LSM with gathers (Clapp et al., 2005) remains a challenge for large scale applications.

In this work, we describe a general framework for iterative LSM with angle domain common image gathers. We derive the numerical solution of LSM in the common image subsurface offset domain and formulate its conjugate gradient inversion scheme with a split Bregman iterations to impose sparsity constraints. When compared to migration in both synthetic and field data, and demonstrate that the proposed algorithm can produce high-resolution angle gathers. We also show that the iterative LSM enhances the angle range by balancing the amplitudes and improving illumination.

**Theory**

We consider seismic data $D(\boldsymbol{x_r}; \boldsymbol{x_s}; \omega)$ in angular frequency $\omega$ with the shot at $\boldsymbol{x_s} = (x_s, y_s, z_s = 0)$ and receiver at $\boldsymbol{x_r} = (x_r, y_r, z_r = 0)$ and assume regular surface sampling and infinite recording aperture. Wave-equation migration (WEM) is able to provide an image by the downward extrapolation of the source wavefield $P_D$ with the designatured zero phase source wavelet $f(\omega)$ (Claerbout, 1971, Valenciano et al., 2011):

$$\begin{cases} (\partial_z + \mathrm{i}\Lambda) P_D(\boldsymbol{x}; \boldsymbol{x_s}; \omega) = 0, \\ P_D(\boldsymbol{x}, 0; \boldsymbol{x_s}, 0; \omega) = \delta(\boldsymbol{x} - \boldsymbol{x_s}) f(\omega), \end{cases} \quad (1)$$

and the upgoing extrapolation of the receiver wavefield $P_U$:

$$\begin{cases} (\partial_z - \mathrm{i}\Lambda) P_U(\boldsymbol{x}; \boldsymbol{x_s}; \omega) = 0, \\ P_U(\boldsymbol{x}, 0; \boldsymbol{x_s}, 0; \omega) = D(\boldsymbol{x_r}; \boldsymbol{x_s}; \omega), \end{cases} \quad (2)$$

We extend the imaging condition with a directional space shift at the subsurface locations $\boldsymbol{x} = (x, y, z)$ to create prestack subsurface offset domain common image gathers (ODCIG) $r(\boldsymbol{x}, \boldsymbol{h})$:

$$r(\boldsymbol{x}, \boldsymbol{h}) = \iint \frac{P_U(\boldsymbol{x} + \boldsymbol{h}) P_D^H(\boldsymbol{x} - \boldsymbol{h})}{\langle P_D(\boldsymbol{x} - \boldsymbol{h}) P_D^H(\boldsymbol{x} - \boldsymbol{h}) \rangle_{\boldsymbol{x}} + \epsilon} \, d\omega \, d\boldsymbol{x_S}. \quad (3)$$

Here, $\partial_z$ denotes the partial derivative respect to $z$; $\Lambda$ is the extrapolation operator; $\boldsymbol{h} = (h_x, h_y)$ denotes the source-receiver half offset; $\langle \, \rangle_{\boldsymbol{x}}$ denotes the preconditioning of the downgoing wavefield subject to its subsurface location $\boldsymbol{x}$, and $\epsilon(\boldsymbol{x}; \boldsymbol{x_s}; \omega)$ is a stabilization term for the subsurface locations with poor signal energy. The Angle Domain Common Image Gathers (ADCIG) can be obtained by radial-trace transforming the ODCIG in (3) (Fomel, 2011).

The image using this migration process can have imperfections due to acquisition and because equations (1-3) are the adjoint of modeling the reflectivity:

$$r(\boldsymbol{x}, \boldsymbol{h}) = M^T d(\boldsymbol{x_r}; \boldsymbol{x_s}; \omega), \quad (4)$$

where $M$ denotes the (Born) modeling operator. Ideally, we want an inverse to this operator. Least-squares migration (LSM) attempts to achieve this by minimizing a cost function $\mathrm{E}(r)$ combining the total data matching between the recorded data $D(\boldsymbol{x_r}; \boldsymbol{x_s}; \omega)$ and the modeled data $d(\boldsymbol{x_r}; \boldsymbol{x_s}; \omega)$ and a sparsity promotion using $L_1$ Total Variation Regularization (TVR) as follows:

$$\mathrm{E}(r) = \frac{1}{2} \|D - d\|_2^2 + |\lambda_x \partial_x r \quad \lambda_y \partial_y r \quad \lambda_z \partial_z r|_1 \quad (5)$$

Here, $\lambda_x$, $\lambda_y$ and $\lambda_z$ are the regularization scalars for the reflectivity variation to ensure the inversion stability such as non-physical migration swings and better sparsity in the inverted image, and $d = M(r)$ is generated by a Born demigration process adjoint to WEM in equations (1-3) (Duan et.al 2019):

$$\begin{cases} (\partial_z + \mathrm{i}\Lambda) P_D(\boldsymbol{x}; \boldsymbol{x_s}; \omega) = \delta(\boldsymbol{x} - \boldsymbol{x_s}) f(\omega), \\ (\partial_z - \mathrm{i}\Lambda) P_U(\boldsymbol{x}) = -\omega^2 \sum_{\boldsymbol{h}} r(\boldsymbol{x}, \boldsymbol{h}) \, P_D(\boldsymbol{x} + \boldsymbol{h}), \\ d(\boldsymbol{x_r}; \boldsymbol{x_s}; \omega) = P_U(\boldsymbol{x_r}; \boldsymbol{x_s}; \omega). \end{cases} \quad (6)$$

To establish a stable and efficient inversion scheme, we can write the numerical solution of the LSM in equation (5) in an equivalent form with weakly enforced constraints using the Split Bregman iterations (Goldstein and Osher, 2009).



10.1190/segam2020-3427923.1

DOI:10.1190/segam2020-3427923.1

**Least-Squares Wave Equation Migration (LSWEM) Scheme**

Given the recorded data $D$ and source signature $f$, our LSWEM is summarized as follows:

1. Initialize: $r_0 = M^T(D)$ and $d_0 = M(r_0)$
2. For $j = 1,2,3,\ldots$ repeat steps 4-8 and exit with $r = r_j$ if stopping criterion has been met:
3. Calculated the image domain steepest descent direction as $\delta r_j = M^T(D - d_{j-1})$.
4. Compute Polak–Ribière conjugate gradient weighting $\beta_j = \max\left(0, \frac{\int \delta r_j(\delta r_j - \delta r_{j-1})dx}{\int \delta r_j \delta r_j dx}\right)$.
5. Update the conjugate gradient $\delta s_j = \delta r_j + \beta_j \delta s_{j-1}$.
6. Calculated the linear search for a scaler $\epsilon = \frac{\iiint\left(M(\delta s_j)\right)(D-d_{j-1})dx_r\, dx_s\, d\omega}{\sqrt{\iiint\left(M(\delta s_j)\right)^2 dx_r\, dx_s\, d\omega \iiint(D-d_{j-1})^2 dx_r\, dx_s\, d\omega}}$.
7. Conduct regularization if required using the Split Bregman iterations (for example in Duan et.al 2019).
8. Compute modeling for the next iteration: $d_j = M(r_j)$.

**Examples**

In the first example, we perform LSWEM on the Sigsbee2b 2D synthetic dataset. The WEM angle domain common image gathers (ADCIG) using cross-correlation imaging condition in Figure 1a shows unbalanced illumination from the left sedimentary to the subsalt area. Using a deconvolution imaging condition in equation (3), a general improvement of illumination and resolution is achieved in the WEM ADCIG (Figure 1b). On close inspection of Figure 1b there remains some undesired amplitude decay and wavelet distortion at far angles due to the limited acquisition aperture. As shown in Figure 1c, over the entire angle range, the LSWEM has not only balanced angle illumination, but

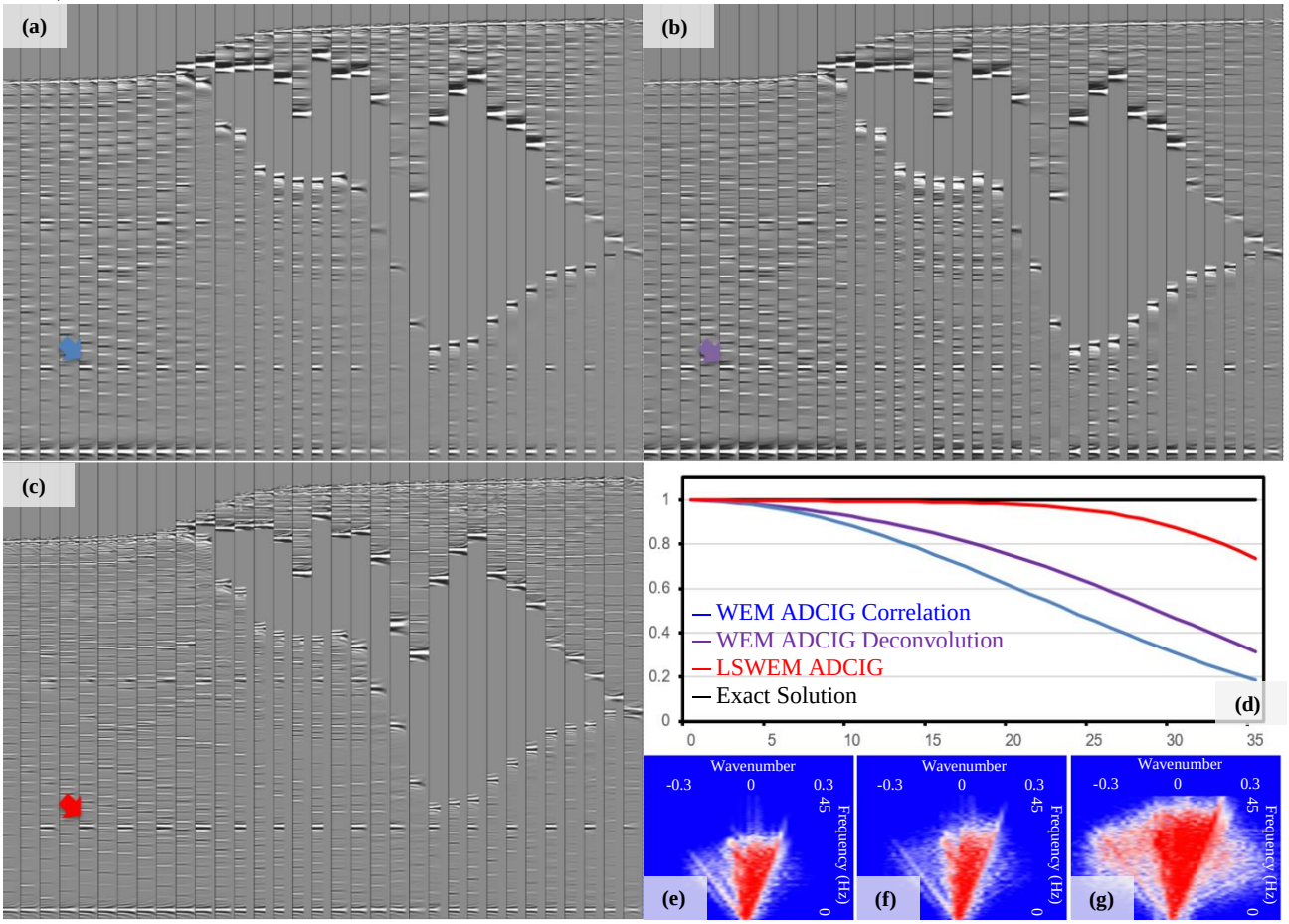


***Figure 1:*** *Sigsbee2b synthetic example: (a) WEM ADCIG with cross-correlation imaging condition; (b) WEM ADCIG with deconvolution imaging condition (3); (c) LSWEM ADCIG; (d) Normalized Amplitude Verse Angle analysis of a typical diffraction point at the arrowed location in (a), (b) and (c); (e) f-k spectrum of a typical angle volume for WEM ADCIG with cross-correlation imaging condition in (a); (f) f-k spectrum of the same angle volume in (e) for WEM ADCIG with deconvolution imaging condition in (b);(g) f-k spectrum of the same angle volume in (e) for LSWEM ADCIG in (c).*



10.1190/segam2020-3427923.1

DOI:10.1190/segam2020-3427923.1

also enhanced resolution by broadening the frequency and wavenumber content (Figure 1e, 1f and 1g). For rigorous analysis without the illumination interference from the salt, we show a normalized amplitude versus angle (AVA) analysis using WEM and LSWEM at a typical diffraction point (arrowed). In Figure 1d, LSWEM is able to recover the constant amplitude behavior off the ADCIG.

We also applied the LSWEM to a narrow azimuth (NAZ) data acquired on Santos Basin, offshore Brazil in 2000. The acquisition consists of 10 streamers with 100 m separation and 8 km length.

The comparison between the angle stacks from WEM (Figure 2a) and LSWEM (Figure 2b) indicates improvement throughout the section, with enhanced postsalt imaging of faults and cap rocks, better imaging of internal salt structures, and refined imaging of reservoir sequence in the presalt section. Note the improved resolution, especially for the cross-cutting fault structure near the top salt body (highlighted by the arrowed crossline range). The F-K spectra clearly illustrate that point (Figures 2c and 2d). Due to the structure of the top salt, the base and presalt events are not evenly illuminated (arrowed location), as it can be observed in the WEM image (Figure 2a). LSWEM successfully recovered the illumination bias, producing an amplitude balanced base salt and presalt section (Figure 2b).

In Figure 3, we present ADCIGs using WEM and LSWEM from the left side of the subline section in Figure 2. It shows similar spatial resolution improvements, in the postsalt section, to those highlighted on the stacked images (Figure 2). In particular, the LSWEM produces a balanced amplitude from near to the far angles. In the presalt section, the enhanced resolution and amplitude balancing over the angles in the LSWEM ADCIG should improve the AVA interpretation of the reservoir. At the base salt (arrowed location in Figure 3), the improvement of the illumination can be observed in the angle gathers (Figure 3b).

To demonstrate the consistent enhancement in amplitudes over subsurface angle, we present the common angle images for near (10°), mid (20°), and far (30°) angles in Figure 4. While WEM provides reasonable angle coverage postsalt, the angle illumination is far from desirable in the presalt. After LSWEM, the consistency of the near, mid and far angles improves. LSWEM reduces the amplitude bias generated in the salt and increases the confidence for further AVA analysis and interpretation, which is key to presalt reservoir characterization.

## Conclusions

Iterative Least-Squares Migration (LSM) produces high-resolution images with reliable AVA response in complex media by reducing the illumination bias on the angular reflectivity. Both synthetic and field data experiments demonstrate that our angle domain iterative LSM implementation can improve the structural continuity, recover image details, extend the consistency in amplitude over the subsurface angle range and improve angle domain amplitude balancing and illumination.

## Acknowledgments

We thank PGS's Multi-Client for providing the datasets and our colleagues for their discussion and support, especially Bertrand Caselitz, Elena Klochikhina, Mikhail Orlovich and Dan Whitmore.

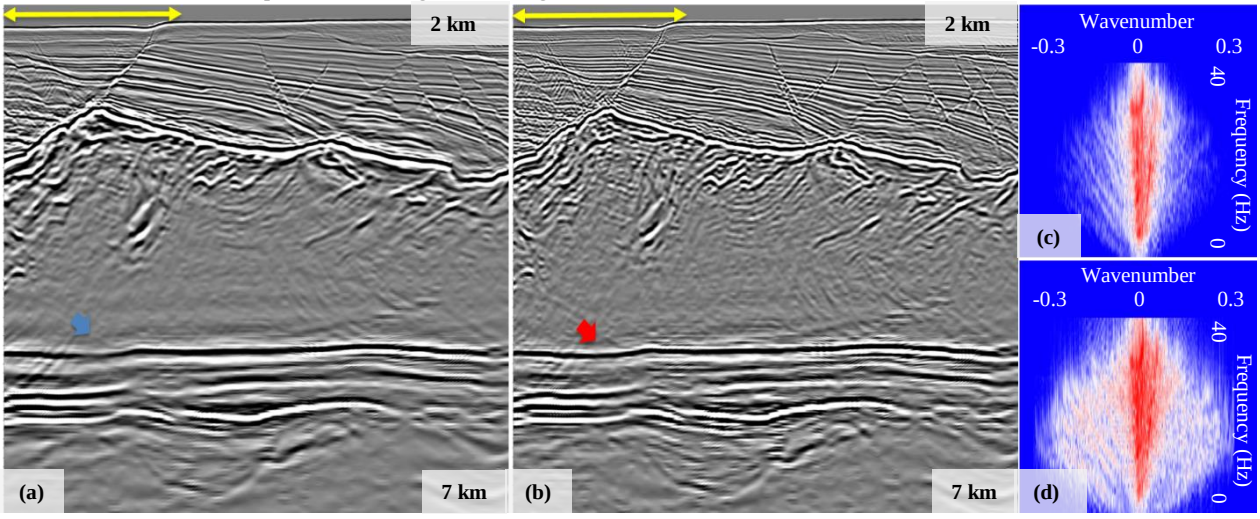


***Figure 2:*** *Santos Basin field example: (a) stacked WEM image using ADCIG; (b) stacked LSWEM image using ADCIG; (c) f-k spectrum of figure (a); (f) f-k spectrum of figure (b).*

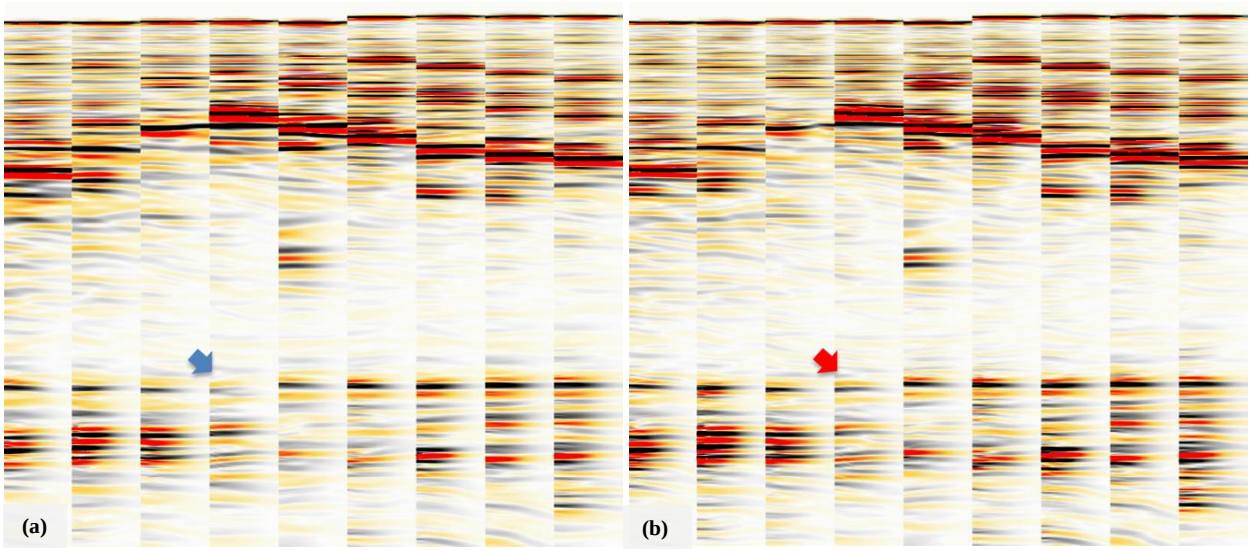


***Figure 3:*** *Santos Basin field example: (a) WEM ADICG at evenly selected crosslines for the left half of figure (2a); (b) LSWEM ADICG for the same crosslines in (3a) for the left half of figure (2b).*

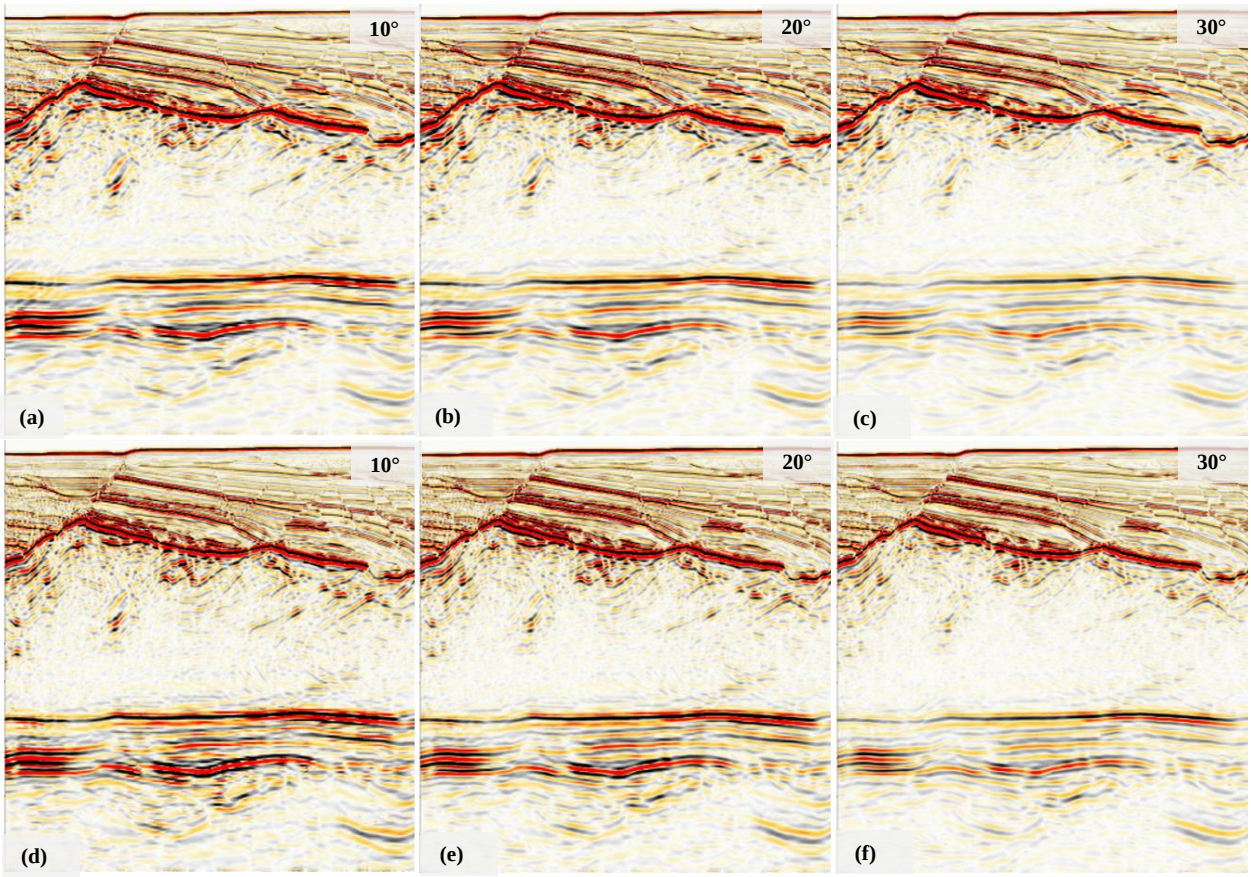


***Figure 4:*** *Santos Basin field example: (a) WEM 10° common angle image; (b) WEM 20° common angle image; (c) WEM 30° common angle image; (d) LSWEM 10° common angle image; (e) LSWEM 20° common angle image; (f) LSWEM 30° common angle image.*

## REFERENCES


Claerbout, J. F., 1971, Toward a unified theory of reflector mapping: Geophysics, **36**, 467–481, doi: https://doi.org/10.1190/1.1440185.

Clapp, M. L., R. G. Clapp, and B. L. Biondi, 2005, Regularized least-squares inversion for 3-D subsalt imaging: 75th Annual International Meeting, SEG, Expanded Abstracts, 1814–1817, doi: https://doi.org/10.1190/1.2148054.

Duan, L., D. Whitmore, N. Chemingui, and E. Klochikhina, 2020, High-resolution angle gathers from iterative least-squares migration: 82nd EAGE Conference and Exhibition.

Fomel, S., 2011, Theory of 3-D angle gathers in wave-equation seismic imaging: Journal of Petroleum Exploration and Production Technology, **1**, 11–16, doi: https://doi.org/10.1007/s13202-011-0004-8.

Guitton, A., 2004, Amplitude and kinematic corrections of migrated images for nonunitary imaging operators: Geophysics, **69**, 1017–1024, doi: https://doi.org/10.1190/1.1778244.

Goldstein, T., and S. Osher, 2009, The split Bregman method for L1-regularized problems: SIAM Journal on Imaging Sciences, **2**, 323–343, doi: https://doi.org/10.1137/080725891.

Valenciano, A. A., N. Chemingui, D. Whitmore, and S. Brandsberg-Dahl, 2011, Wave equation migration with attenuation compensation: 73rd EAGE Conference and Exhibition.

Valenciano, A. A., M. Orlovich, E. Klochikhina, and N. Chemingui, 2019, Least-squares migration with gathers: 89th Annual International Meeting, SEG, Expanded Abstracts, 4206–4210, doi: https://doi.org/10.1190/segam2019-3216342.1.